Available online at www.sciencedirect.com
SCIENCE DIRECT®
Journal of Power Sources 119–121 (2003) 106–109
JOURNAL OF POWER SOURCES
www.elsevier.com/locate/jpowsour

Sn–Zr–Ag alloy thin-film anodes

Young-Lae Kim[a], Seung-Joo Lee[b], Hong-Koo Baik[b], Sung-Man Lee[a,*]

[a]*Department of Advanced Material Science and Engineering, Kangwon National University, Chuncheon, Kangwon-Do 200-701, South Korea*
[b]*Department of Metallurgical Engineering, Yonsei University, Seoul 120-749, South Korea*

Abstract

Sn–Zr and Ag-doped Sn–Zr thin films were prepared by an electron-beam evaporation method using pure separate metal sources. Electrochemical cycling performance was obtained as a function of film composition. The cycling stability of Sn–Zr film electrodes increased with Zr content. An Ag-doped Sn–Zr thin film such as $Sn_{57}Zr_{33}Ag_{10}$ showed excellent cycling stability and capacity retention. The composition dependence on electrochemical behavior is related to the microstructural changes in the films.

Keywords: Anode film; Microbattery; Sn–Zr; Sn–Zr–Ag alloys; Cycling performance

1. Introduction

Lithium metal has commonly been used or proposed as anodes for rechargeable thin-film microbatteries which can be employed as power sources for microdevices. However, lithium metal has some problems for the application due to its low melting point (181 °C), high reactivity with air, and tendency to form dendrites. Hence, there is currently a significant interest in finding new anode materials [1–3].

Alloy-based materials containing such lithium storage metals as Al, Si and Sn have been extensively studied as anodes for lithium-ion batteries. However, these alloy systems undergo large volume changes during Li insertion/extraction cycling [4–6]. This limits the mechanical stability and cycle life of the electrode. Recently, intermetallic compounds or alloys AM have been widely studied, where A is an "active" alloying element and M is an "inactive" element [7,8]. The performance of alloy electrodes can be improved significantly when the active alloying elements are finely dispersed with an inactive component in a composite matrix. In addition, intermetallic alloys, such as Cu_6Sn_5 show improved electrochemical cycling performance compared to pure Sn [9]. In general, the reaction of these intermetallic compounds with lithium results in a displacement reaction in which the intermetallic compounds are decomposed to produce inactive metallic component and a lithium–tin composite alloy. On cycling, the aggregation of Sn regions to larger clusters results in capacity fade [10]. It is expected, however, that the strong affinity between Sn and the inactive atoms might suppress agglomeration of Sn during cycling and accommodate lithium with relatively small volume change by limiting Li_xSn alloy formation. The Sn–Zr system was selected here because it has the large negative values of the enthalpy of formation (ΔH_f) compared with the Sn–Li system, as estimated by the method proposed by Nam et al. [11].

In order that the above concept is feasible, it is necessary to prepare an optimized alloy film with a homogeneous distribution of constituents. From the low melting point of Sn, however, it seems inevitable that the precipitation of Sn occurs during the deposition by co-evaporation method used in this work, especially for Sn-rich Sn–Zr alloy system. As mentioned above, this may result in a poor long-term cycling stability due to the large volume changes of Sn precipitates which occur during lithiation and delithiation. These shortcomings could be overcome by using the ternary system Sn–Zr–Ag, in which the Sn–Ag alloying could probably exclude the formation of metallic Sn precipitates. Besides, as Ag is active towards Li, the addition of Ag would not limit the Li storage capacity of the Sn-based alloys differently from being expected from Zr doping. Sn–Ag alloys have been also studied as anodes for Li-ion batteries [12].

In this study, the Sn–Zr and Ag-doped Sn–Zr thin films were synthesized and characterized by X-ray diffraction (XRD) and electrochemical measurements.

* Corresponding author. Tel.: +82-33-250-6266; fax: +82-33-242-6256.
E-mail address: smlee@kangwon.ac.kr (S.-M. Lee).

0378-7753/03/$ – see front matter © 2003 Elsevier Science B.V. All rights reserved.
doi:10.1016/S0378-7753(03)00134-4

2. Experimental

Sn–Zr and Ag-doped Sn–Zr thin films were deposited on a 12 mm diameter Cu substrate by an electron-beam evaporator from separate pure metal sources. The film thickness was controlled by the evaporation time and measured by using a surface profilometer. The composition analysis for the films was carried out by energy dispersive X-ray spectroscopy (EDS) analysis. The surface microstructure was determined by field-emission scanning electron microscopy (FESEM) and X-ray diffraction (XRD) experiments were carried out with Cu Kα radiation.

CR2016 coin cells were fabricated to test the electrochemical properties of thin-film electrodes. The cells were assembled in an argon filled glove-box. The electrolyte was 1 M $LiPF_6$ in a mixture of ethylene carbonate (EC) and diethyl carbonate (DEC) (1:1 by volume, Cheil Industries Inc., Korea). All cells were tested at 30 °C at a constant current of 30 μA/cm^2 in the voltage range 0.0–1.2 V versus Li/Li$^+$.

3. Results and discussion

The XRD patterns of the Sn–Zr thin films as a function of composition are given in Fig. 1. Peaks marked with S correspond to the Cu substrate. Peaks corresponding to Sn appeared in Sn-rich film, but the peaks broadened and their intensities decreased significantly with increasing Zr content in the film. No crystalline peak indicates that the film is in the XRD amorphous state. Fig. 2 shows the FESEM images of the films. Element maps of Sn and Zr using EDS (data not shown here) conformed that the Sn particles were agglomerated. It appears that particle size decreases and the distribution becomes more uniform as Zr content increases. The Zr-rich film of $Sn_{30}Zr_{70}$ shows a very smooth surface morphology (Fig. 2(d)). This is consistent with the decrease of XRD peak intensities of Sn with increasing Zr content in the film. Fig. 3 shows the first cycle profiles for Sn–Zr thin-film electrodes. In the Sn-rich sample $Sn_{82}Zr_{18}$, the potential plateaus in the voltage profile are noticeable. With increasing Zr content film, the voltage profile becomes very smooth. This is more evident in the differential capacity versus voltage for the same cells, as shown in Fig. 4. The plateaus visible in Fig. 3 appear as sharp peaks which are indicative of the formation of bulk-like Li–Sn alloys. In contrast, the differential capacity for the Zr-rich sample $Sn_{44}Zr_{56}$ shows a rather smooth curve, which is stable during cycling. It is also

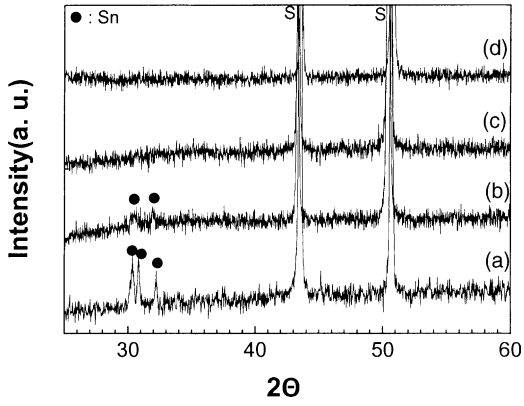

Fig. 1. XRD patterns of the Sn–Zr thin films as a function of composition: (a) $Sn_{82}Zr_{18}$, (b) $Sn_{62}Zr_{38}$, (c) $Sn_{44}Zr_{56}$, (d) $Sn_{30}Zr_{70}$.

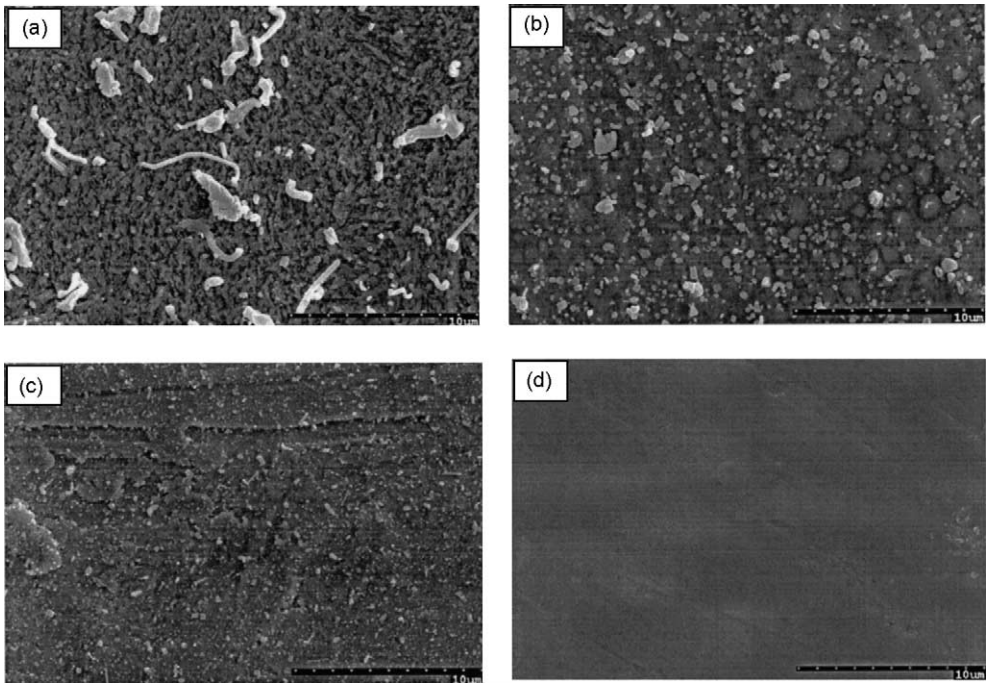

Fig. 2. FESEM images of Sn–Zr thin films: (a) $Sn_{82}Zr_{18}$, (b) $Sn_{62}Zr_{38}$, (c) $Sn_{44}Zr_{56}$, (d) $Sn_{30}Zr_{70}$.

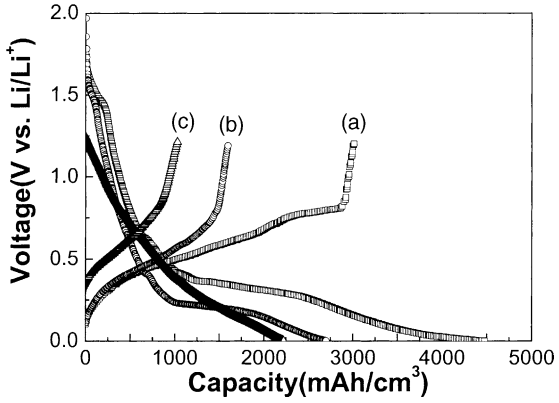

Fig. 3. The first cycle profiles for Sn–Zr thin-film electrodes: (a) $Sn_{82}Zr_{18}$, (b) $Sn_{62}Zr_{38}$, (c) $Sn_{44}Zr_{56}$.

found that the initial charge capacity decreases with increase of Zr in the film (see Fig. 3). Therefore, alloying of Sn with Zr limits the amount of lithium alloying with Sn to form Li_xSn alloys, resulting in reduction of capacity. A relatively strong affinity between Sn and Zr atoms may prevent Sn from aggregation into larger clusters, which leads to a good capacity retention during cycling. Fig. 5 shows the capacity versus cycle number for Sn–Zr thin films. The cycling performance is improved by the addition of Zr. In particular, the Zr-rich sample ($Sn_{30}Zr_{70}$) shows the excellent cyclability, but its capacity is quite small.

This indicates that the alloying of Sn with Zr decreases the volume expansion and buffers the volume changes of the active phase, which leads to the stabilization of the alloy film electrode, as expected. However, this results in the reduction of capacity. Sn-rich alloy systems, exhibiting an increased capacity, also show the declining capacities during long-term cycling due to the aggregation of Sn. Moreover, these Sn-rich films appeared to have the aggregated Sn particles even in as-deposited state as shown in Fig. 2.

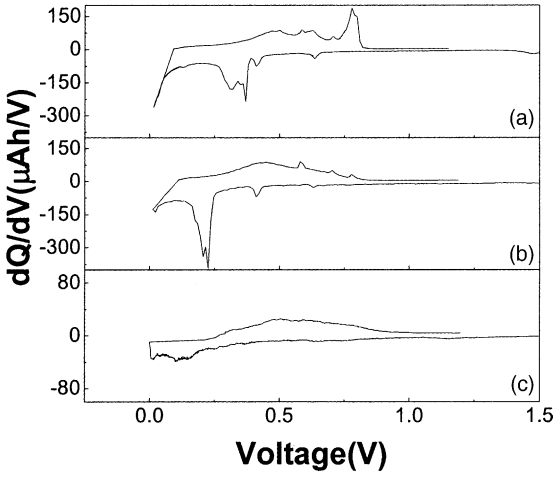

Fig. 4. The differential capacity vs. voltage for first cycle of the Sn–Zr thin-film electrodes: (a) $Sn_{82}Zr_{18}$, (b) $Sn_{62}Zr_{38}$, (c) $Sn_{44}Zr_{56}$.

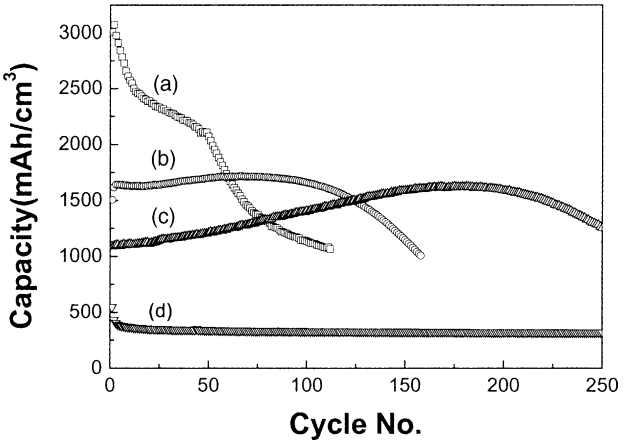

Fig. 5. The capacity vs. cycle number for Sn–Zr thin-film electrodes: (a) $Sn_{82}Zr_{18}$, (b) $Sn_{62}Zr_{38}$, (c) $Sn_{44}Zr_{56}$, (d) $Sn_{30}Zr_{70}$.

Here, we have prepared the Ag-containing Sn–Zr films to retard the aggregation of Sn according to the background mentioned before. Fig. 6 gives the cyclability of Sn–Zr–Ag alloy thin-film electrodes. We note that the atomic ratio of

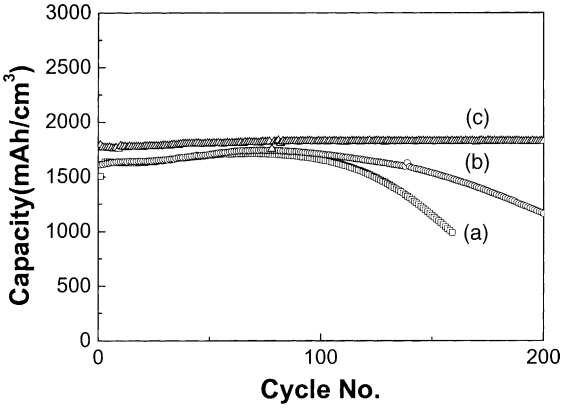

Fig. 6. The capacity vs. cycle number for Sn–Zr–Ag alloy thin-film electrodes: (a) $Sn_{62}Zr_{38}$, (b) $Sn_{64}Zr_{34}Ag_2$, (c) $Sn_{57}Zr_{33}Ag_{10}$.

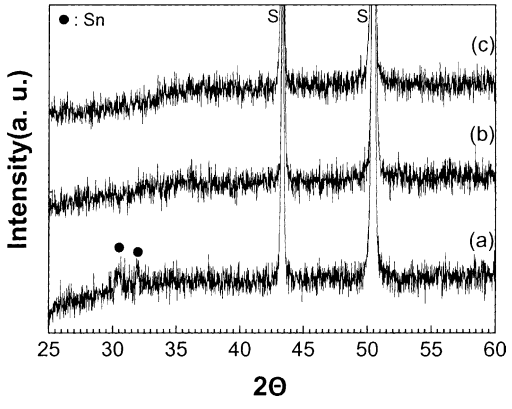

Fig. 7. The XRD patterns of Ag-containing Sn–Zr films: (a) $Sn_{62}Zr_{38}$, (b) $Sn_{64}Zr_{34}Ag_2$, (c) $Sn_{57}Zr_{33}Ag_{10}$.

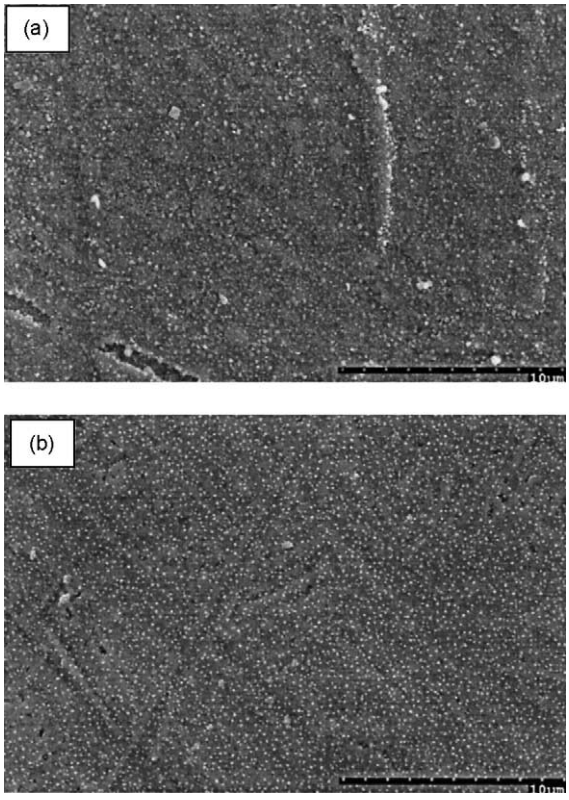

Fig. 8. The FESEM images of Sn–Zr–Ag alloy thin-film electrodes: (a) $Sn_{64}Zr_{34}Ag_2$, (b) $Sn_{57}Zr_{33}Ag_{10}$.

Sn to Zr in the Ag-doped films is comparable to that of the undoped sample. The cycling performances of Ag-containing Sn–Zr films are better than those of corresponding Sn–Zr samples. In particular, the electrode containing 10 at.% Ag ($Sn_{57}Zr_{33}Ag_{10}$) exhibited a stable capacity retention for many cycles. It seems likely that the excellent stability of the Ag-doped electrode may be attributed to the existence of very finely dispersed Sn within the matrix. The XRD patterns of Ag-containing Sn–Zr films are shown in Fig. 7. For comparison, the XRD pattern of the Sn–Zr film with a comparable ratio of Sn–Zr is also shown. For Ag-doped samples, even for the film containing 2 at.% Ag, the diffraction lines of Sn cannot be distinguished. SEM indicates that the morphology of the Sn–Zr film has been substantially modified by Ag-doping (see Fig. 8). The Ag-doped films in Fig. 8 show a fine and uniform distribution of the Sn aggregated particles compared with that of the undoped sample in Fig. 2(b). Ag-containing Sn–Zr films therefore appear to be promising as an anode material for thin-film micorbatteries.

4. Conclusions

Sn–Zr and Sn–Zr–Ag thin films have been prepared using an electron-beam evaporator and compared in terms of the electrochemical cycling performance as a function of film composition. For Sn–Zr thin films, cyclability is improved with the addition of Zr, although capacity then decreases. The cycling stability of Sn–Zr thin-film electrodes appear to be significantly increased by doping the film with Ag.

Acknowledgements

This work was supported by the Korean Ministry of Science and Technology through the research program for "National Research Laboratory".

References

[1] J. Yang, M. Winter, J.O. Besenhard, Solid State Ionics 90 (1996) 281.
[2] J.O. Besenhard, J. Yang, M. Winter, J. Power Source 68 (1997) 87.
[3] B.A. Boukamp, G.C. Lesh, R.A. Huggins, J. Electrochem. Soc. 133 (1986) 457.
[4] M. Winter, J.O. Besenhard, Electrochim. Acta 45 (1999) 31.
[5] O. Mao, R.A. Dunlap, I.A. Courtney, J.R. Dahn, J. Electrochem. Soc. 145 (1998) 4195.
[6] K.D. Kepler, J.T. Vaughey, M.M. Thackeray, Electrochem. Solid-State Lett. 2 (1999) 307.
[7] O. Mao, J.R. Dahn, J. Electrochem. Soc. 146 (1999) 414.
[8] A.R. Miedema, Philips Tech. Rev. 36 (1976) 217.
[9] J.B. Bates, N.J. Dudney, B. Neudecker, A. Ueda, C.D. Evans, Solid State Ionics 135 (2000) 33.
[10] S.J. Lee, H.Y. Lee, T.S. Ha, H.K. Baik, S.M. Lee, Electrochem. Solid-State Lett. 5 (2002) A138.
[11] S.C. Nam, Y.S. Yoon, W.I. Cho, B.W. Cho, H.S. Chun, K.S. Yun, Electrochem. Commun. 3 (2001) 6.
[12] M. Wachtler, M. Winter, J.O. Besenhard, J. Power Source 105 (2002) 151.